JOURNAL OF CATALYSIS **172,** 463–470 (1997)
ARTICLE NO. CA971903

Pumice-Supported Nickel Catalysts

Structural and Reactivity Study in the Hydrogenation of CO

A. M. Venezia,*,†,[1] A. Parmaliana,‡,§ A. Mezzapica,§ and G. Deganello*,†

*Dipartimento di Chimica Inorganica, Università di Palermo, Via Archirafi 26-28, 90123 Palermo, Italy; †Istituto di Chimica e Tecnologia dei Prodotti Naturali (CNR), Via Ugo La Malfa 153, 90146, Palermo, Italy; ‡Dipartimento di Chimica Industriale, Università degli Studi di Messina, Salita Sperone c.p. 29, I-98166 S. Agata (Messina), Italy; and §Istituto CNR-TAE, Salita S. Lucia 39, 98126, Messina, Italy

Received January 21, 1997; revised April 25, 1997; accepted July 24, 1997

A series of nickel catalysts supported on pumice was prepared by precipitation and impregnation techniques. The influence of the calcination and reduction temperatures on the structural properties such as lattice parameters and particle dimensions of the oxide precursors and of the reduced catalysts was investigated by X-ray diffraction measurements. The effect of structural changes on the catalytic activity in the hydrogenation of carbon monoxide has been evaluated. The turnover frequencies, as well as product distributions, are discussed in terms of the influence of the support properties and of its interaction with the metal. Changes of the C_{2+} yield over CH_4 yield ratio versus nickel dispersion are attributed to the presence of the alkali ions in the support structure. The catalytic performance of the catalysts does not change after 15–18 h time on stream. Indeed, the X-ray diffraction and photoelectron spectroscopy analysis of the catalysts, before and after reaction, excluded sintering of the metal particle, as well as coke formation.

INTRODUCTION

Supported nickel catalysts are widely used in CO hydrogenation. Formation of methane and higher hydrocarbons, very important for the production of synthetic fuel, has been studied in great detail from the kinetic point of view. The reaction has been considered in many studies as structure insensitive (1, 2), but the supports interacting with the metal are shown to have an important role (3–5). The carrier affects the catalytic properties of the supported metal either because, in the presence of a structurally sensitive reaction it promotes dispersion of the metal, or because of the so-called SMSI (strong metal-support interaction) effects (6, 7). Results from surface studies on nickel single-crystals have revealed that the methanation reaction is structure insensitive (8); that is, the coordination number of a particular atomic site, either a corner, edge, or planar atom, does not affect the reactivity of the site itself. Moreover, data on Ni/Al_2O_3, Ni/TiO_2 catalysts provided evidence that strong metal-support interactions increase the activity of nickel for CO hydrogenation (4).

The addition of promoters such as alkali metals to nickel catalysts improves the selectivity toward alkenes and higher hydrocarbons (9–11). They decrease the hydrogen chemisorption capacity of the transition metal and, therefore, by reducing the rates of hydrogenation, allow for more carbon–carbon bond formation before the desorption of the hydrocarbon products (12–14). From ferromagnetic measurements and temperature programmed hydrogenation, it was shown that alkali promotion produces a marked increase of carbon deposits interacting with metallic nickel and forming surface and bulk carbides (11, 15). This accumulation of carbon was explained either with an increase of the rate of CO dissociation or (and) with a decrease in the rate of hydrogenation and would be directly related to the observed change of selectivity, particularly an increase of the C_{2+} hydrocarbon formation. In order to reduce the formation of carbon, causing serious problems in the reactors, a poisoning agent for the coking reaction, such as sulphur or copper, is added (16, 17). Studies on Ni/SiO_2 and $Ni/Cu/SiO_2$ catalysts indicated that the carbon formation and the methanation reaction have different rate-controlling steps (18). The disproportion of adsorbed CO is rate-controlling in the carbon formation, whereas the hydrogenation of CH surface species is the rate-controlling step in the methanation reaction (19, 20).

A recent study on the morphological changes and deactivation mechanism of alkali-promoted Ni/SiO_2 in CO hydrogenation indicated that the alkali ions, at least when the atomic ratio Alkali/Ni does not exceed 0.15, prevent nickel sintering. The role of the alkali ions would be to reduce the mobility of subcarbonyl species $Ni(CO)_x$, therefore slowing down the process of sintering (10).

Pumice, an aluminosilicate naturally doped with alkali ions, has been recently used as support for Pd catalysts

[1] Corresponding author. E-mail: anna@ictpn.pa.cnr.it.

0021-9517/97 $25.00

(21, 22). The improved catalytic properties of these catalysts, in the hydrogenation of alkadienes (23) and alkynes (24, 25) over an extended range of metal particle dispersions, was attributed to an increased electron density of the Pd atoms interacting with the support (26). A Fourier transform infrared study of CO on supported palladium catalysts illustrated the role of alkali metal ions being part of the support structure (27). The electronic charge transfer from the support to the palladium atoms, shown by the X-ray photoelectron spectroscopy studies (XPS), produced a decrease in intensity and a shift toward lower frequencies of the IR spectra bands of the chemisorbed CO. Both these effects, increasing with the increase of the Na/Pd atomic ratio, were attributed to an electron charge transfer to the supported metal (27). The down-field shift is due to the electron transfer from the metal to the π^* molecular orbitals of CO and the reduced intensity being a consequence of a decreased Pd $\leftarrow$ CO σ-type interaction.

Based on the above results and on the finding of a preliminary XPS study of pumice-supported nickel catalysts indicating a preferential interaction of nickel with the alumina component (28), a series of nickel catalysts supported on pumice were prepared and characterized. To investigate for possible influence of the catalyst precursors, two preparation procedures were followed; deposition–precipitation and ion exchange. The hydrogenation of carbon monoxide was used as a test reaction and the catalytic behavior was related to structural properties of the catalysts being changed by using different calcination and reduction temperatures.

EXPERIMENTAL

Catalysts Preparation

Pumice, obtained from Pumex Spa in Lipari, Italy, is characterized by a specific surface area of 5–7 $m^2 g^{-1}$ (21). Following a previous procedure, it was purified by treatment with diluted HNO_3 before being used as support (21). The acid treatment did not affect the specific surface area, but slightly depleted the amount of sodium, potassium, and aluminum, yielding a pumice of the following composition: $SiO_2 = 87.7$ wt%, $Al_2O_3 = 7.0$ wt%; $Na_2O = 2.0$ wt%; $K_2O = 3.3$ wt%, as determined by atomic absorption analysis. Possible structural and chemical changes of the support, occurring at the high temperature used for the calcination of the catalysts have been checked by X-ray diffraction analysis: according to the wide angle (WAXS) measurements the high temperature did not change the amorphicity of the support; from small angle measurements (SAXS), only a slight increase in the specific surface area of the support (not appreciable with the BET analysis) was determined upon calcination at the highest temperature of 1273 K, probably due to loss of structurally bound water. As shown previously by XPS technique (28), the increased temperature induced surface segregation of the alkali ions.

One series of catalysts was prepared by a homogeneous deposition–precipitation method developed by Van Dillen *et al.* for Ni on silica (29); the method involved thermal decomposition of urea to CO_2 and ammonium hydroxide, and the subsequent precipitation of nickel hydroxide which slowly deposited on the hydroxylic sites of the pumice support (28). The other series labeled with (E) was obtained by the ion-exchange method involving an exchange of the cation complex $[Ni(NH_3)_6]^{2+}$, formed in an ammoniacal solution of $Ni(NO_3)_2 \cdot 6H_2O$, with the acidic protons of the support surface. Both methods produced good dispersion of the nickel particles. The precursors were then calcined overnight at different temperatures. Subsequently they were reduced under a hydrogen flow of 30 cm^3/min at various temperatures with a heating rate of 10 K/min. The samples were kept at the desired temperature for 8 h and then slowly cooled down to room temperature. The completeness of the reduction process was checked by temperature programmed reduction (TPR) performed on the samples after the hydrogen treatment described above. The X-ray diffractograms of the samples before and after reduction were typical of NiO and nickel metal, respectively. Only the sample which was calcined at 1273 K still contained some unreduced nickel oxide and nickel–silica antigorite phase (28). The nickel concentration was determined by atomic absorption spectroscopy with an accuracy of $\pm 10\%$.

Catalytic Tests

The activity and stability of pumice-supported nickel catalysts in carbon monoxide hydrogenation have been evaluated at 533 K by a continuous flow fixed-bed microreactor ($l = 100$ mm, ID = 4 mm) operating at atmospheric pressure. The reaction mixture, consisting of CO (30% vol), H_2 (60% vol), and N_2 (10% vol) as standard for GC, was fed into the reactor containing the catalyst ($W_{cat} = 0.25$ g; 40–70 mesh) with a flow rate of 30 STP cm^3/min (GHSV = 7200 h^{-1}). Prior to each test the catalyst was reduced *in situ* at 673 K under hydrogen flow (30 STP cm^3/min) for 1 h (heating rate = 10 K/min), then conditioned to reaction temperature under the H_2 atmosphere. The extent of CO conversion (mol%) was taken as a measure of the catalytic activity. In order to obtain reliable turnover frequency (TOF s^{-1}) data, a series of experiments under differential conditions (CO conv. <10 mol%) were carried out. The absence of any influence of diffusion effects under operating conditions was adequately checked. Reactants and reaction products were analysed by on-line GC (Dani 3800 instrument) equipped with a two-column analysis system (i) Porapack QS column (80–100 mesh); *l*, 2.5 m; ID, 4 mm) and (ii) Molecular Sieves SA (80–100 mesh; *l*, 2.5 m; ID, 4 mm).

Structural Characterization

The X-ray diffraction measurements were performed with a Philips X-ray diffractometer using Cu Kα radiation, as described previously (28). The metal particle sizes of the reduced catalysts were estimated as volume-average crystallite dimension, through the line broadening (LB) of the (111) and (200) peaks using the Scherrer equation according to the method reported in the literature (30).

TPR measurements of selected samples in the temperature range 373–1073 K were carried out in a linear quartz reactor using a 5% H_2/N_2 mixture flowing at 40 STP cm^3 min^{-1} and using a heating rate of 15 K min^{-1}. The H_2 consumption was monitored by a TCD (thermoconductivity detector) connected to a personal computer for data storage and processing. The TCD was calibrated quantitatively, for the whole temperature range investigated, using known amounts of Ni(II), Cu(II), and Sn(IV) oxides. Deconvolution of the experimental reduction profile was performed using a nonlinear least-squares fitting.

X-ray photoelectron spectra of the C 1s core level and of the Ni 2p and Si 2p levels of the catalysts before and after reaction were measured with a Perkin-Elmer PHI 5600-ci photoelectron spectrometer using monochromatized Al Kα radiation (1486.6 eV). Details of the experimental apparatus were previously given (28).

RESULTS AND DISCUSSION

Structural Study

In Table 1 the various samples are listed, along with their calcination and reduction temperatures, the XRD derived nickel particle sizes, and the corresponding dispersions. Catalysts with 7.5 and 4 wt% nickel, prepared with the deposition–precipitation method, and with 1.5 wt% nickel, prepared by ion exchange, are reported. The dispersions were obtained from the equation given by Smith *et al.* (31), assuming a spherical shape for metal particles:

$$D = 101/d \text{ (nm)}.$$

By comparing the samples with the same thermal treatments, in agreement with previous study on various supports, a larger dispersion is generally achieved for small metal content (32). Based on the thermal treatments, the catalysts may be classified into two groups: one obtained by varying the calcination temperature, T_C, and reducing them at the same temperature; and the other using a fixed calcination temperature and changing the reduction temperature, T_R. In both cases the increase of the temperature induces sintering of the particles with the larger effect caused by the reduction temperature. Since a high calcination temperature in the presence of a strong metal–support interaction usually causes a redispersion of the metal oxide (33) yielding smaller metal particles, the present results suggest that the interaction between Ni(II) and pumice, revealed previously by an XPS study, is rather weak. Moreover, the nickel atoms forming after reduction are quite mobile, since they can be easily sintered at temperatures much below the melting point of the nickel.

TABLE 1

Samples Treated at Different Calcination Temperatures T_C and Different Reduction Temperatures T_R with the Corresponding Particle Diameters, d, Percentage Dispersions, D, and Unit Cell Parameters *a* of the Nickel Metal Phase

Catalyst	T_C (K)	T_R (K)	d (Å)	D (%)	*a* (Å)
7.5% NiC6R7	673	773	45	22	3.527
7.5% NiC8R7	873	773	56	18	3.527
7.5% NiC10R7	1073	773	78	13	3.529
7.5% NiC12R7	1273	773	250	4	3.527
4% NiC8R6	873	673	26	39	3.559
4% NiC8R7	873	773	42	24	3.523
4% NiC8R8	873	873	59	17	3.529
1.5% NiC6R7(E)	673	773	32	32	3.543
Ni metal					3.524

Note. The unit cell parameter of the bulk Ni metal is also given.

To further investigate the importance of the calcination step on the final dispersion of the reduced particles, the Sherrer analysis of the X-ray diffractogram patterns of nickel oxide present in the calcined samples was performed. After fitting the experimental (111) and (200) reflection peaks using the instrument-provided software, the LB analysis of the peaks relative to the samples calcined at 873 K resulted in a volume-average crystallite sizes of 28–29 Å. The two corresponding diffractogram regions of the samples calcined at 1073 K contained multiple peaks which were both fitted with two components of different linewidths. The (111) reflection of the sample 7.5% NiC10, fitted with two Gaussian–Lorentzian components, is given in Fig. 1. The LB analysis of each component gave two types of oxide particles, large (1000–1200 Å) and small (33–38 Å). The results for some of the samples calcined at different temperatures are reported in Table 2. The percentage (%)

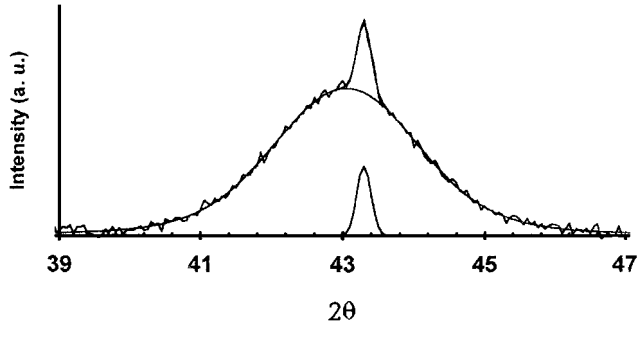

FIG. 1. Fitted and experimental (111) reflection peak of the calcined 7.5% NiC10 catalyst.

TABLE 2

Diameters d and Unit Cell Parameters *a* Corresponding to the Small and Large Nickel Oxide Particles Obtained after Calcination of Some Samples

Catalyst	T_C (K)	d (Å) small	*a* (Å) small	d (Å) large	*a* (Å) large
7.5% NiC8	873	29 (100)	4.201		
7.5% NiC10	1073	38 (96)	4.202	1200 (04)	4.181
4% NiC8	873	28 (100)	4.206		
4% NiC10	1073	33 (88)	4.197	1000 (12)	4.177
NiO bulk					4.177

Note. The percentages of each type of oxide are given in parentheses. The unit cell parameter for bulk NiO is also given.

of differently sized nickel oxide particles, as deduced from the relative intensity of the peak components, are given in parentheses. For all the samples, upon reduction, according to the X-ray diffractograms, monodisperse nickel metal particles are obtained. The attainment of single-sized metal particles may be caused by the mobility of the metal ions and metal atoms on the suface of the supported metal oxides and forming metal particles of one average size determined by the temperature of reduction.

TPR measurements of the 7.5% Ni/pumice catalyst calcined at 673 and 1073 K have been performed in order to ascertain the influence of the calcination temperature on the interaction of the Ni precursor with the matrix of the pumice support. In Figs. 2 and 3 the TPR profiles of the samples calcined at 1073 and 673 K are given. The fitting of the profiles with Gaussian–Lorentzian curves of arbitrary linewidths has only a qualitative character allowing us, however, to evaluate more accurately the temperature of the peak maxima (T_M) listed in Table 3 along with the related peak areas. The complete reduction of the samples treated with H_2 at a temperature below the T_M has been checked by performing a TPR run immediately after the reduction. The flatness of the profile ensured the complete reduction of the samples. The component at higher temperature could be due to Ni(II) species less reducible, owing to

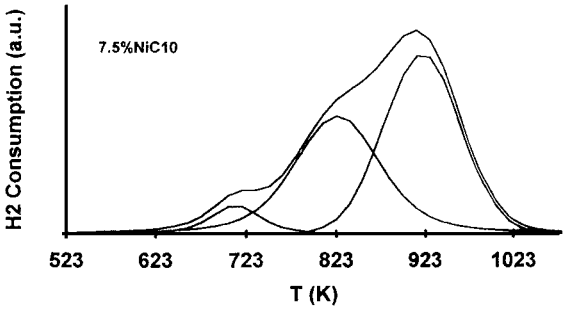

FIG. 2. Temperature-programmed reduction profile of the 7.5% NiC10 catalyst with fitted peaks.

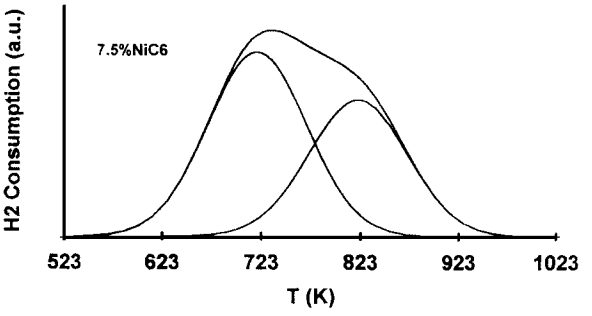

FIG. 3. Temperature-programmed reduction profile of the 7.5% NiC6 catalyst with fitted peaks.

an interaction with the support as proved by previous X-ray diffraction data showing the formation of some nickel–silica antigorite-like structure (28, 34). Notably, the sample calcined at 1073 K shows a reduction peak at 921 K which signals the reduction of a Ni(II) form likely arising from a $NiAl_2O_4$ compound formed by the solid state reaction between the nickel precursor and support. Indeed previous XPS study of pumice-supported nickel catalysts, at the early stage of the preparation, after drying at 383 K, indicated a preferential interaction between nickel and aluminum (28). The calcination treatment at high temperatures may strengthen such interaction, producing a "fixed" oxide detected by the X-ray diffractogram as small NiO particles, along with the large "free" NiO particles (35, 36). From the structural results of Table 2, based on the XRD analysis, it can be concluded that, whereas a low calcination temperature produces, on the average, small oxide crystallites, a high calcination temperature produces small and large crystallites. With increase in temperature the small oxide particles coalesce giving rise to large particles. Such a process of agglomeration is dependent on the nickel loading, as indicated by the percentage of each oxide particle; within the same time and temperature of calcination, a higher percentage of larger particles is obtained with the lower nickel content catalyst. The apparent contradiction between TPR and X-ray results, that is, the fact that larger particles are found in the diffractogram of the catalysts calcined at higher temperature at which more interacting small particles are likely

TABLE 3

TPR Characteristic Peak, T_M, and Relative Area, of the 7.5% Ni/Pumice Samples Calcined at Two Different Temperatures T_C

Catalyst	T_C (K)	T_M (K)	Peak area (a.u.)
7.5% NiC6	673	717	300
		819	222
7.5% NiC10	1073	707	180
		823	180
		921	251

to be formed, is eliminated if one assumes that the calcination temperature, in addition to intensifying the bonding between Ni(II) species and support elements, induces sintering of those particles interacting less with the support. Indeed, following calcination at 1273 K, some unreduced nickel was left after the H_2 treatment, again indicative of a nickel species that is more difficult to reduce (35).

An analysis of the unit cell parameters of the nickel oxide and nickel metallic phase, both of cubic lattice, was performed in order to check for the possible effect of the support on the structures of these phases. The cell parameter *a* was derived from the reflections (111), (200), and (220). A graphical method of extrapolation versus $(1/2)(\cos^2\vartheta/\sin\vartheta + \cos^2\vartheta/\vartheta)$, followed by a least-squares technique was used (30). The reproducibility of the lattice parameter *a* over three measurements was ± 0.005 Å. The parameters relative to the nickel metal and to the nickel oxide phases are given in Tables 1 and 2, along with the corresponding values for the pure metal and oxide. The metal parameter of most of the catalysts is, within the experimental error, the same as the bulk metal value, except for the two samples with particle sizes of 26 and 32 Å having a larger value. This result contrasts with EXAFS studies of small metal particles, reporting a decrease of the lattice parameters due to contraction of the metal–metal bond (37). The formation of multiply twinned particles (MTP), or other lattice disorder, may produce cell expansion and metal–support interaction may contribute to such disorder (38).

As shown in Table 2, whereas the unit cell parameter of the large nickel oxide particles is typical of the NiO bulk phase, larger parameters are found for the small particles. In the absence of any crystal deformation, expansion of the lattice volume of an ionic crystal may take place because of missing ions such as oxygen vacancies (39).

CO Hydrogenation

The catalytic behavior of the Ni/pumice samples in the hydrogenation of CO is presented in Table 4 in terms of CO conversion and selectivity to CH_4, C_{2+}, and CO_2.

TABLE 4

Catalytic Properties of Ni/Pumice Catalysts after 2 h of Reaction

Catalysts	CO conv. (%)	S_{CH_4}	$S_{C_{2+}}$	S_{CO_2}	$TOF(CO) \times 10^2$ (s^{-1})
7.5% NiC6R7	9.7	73.4	25.3	1.3	3.8
7.5% NiC8R7	3.1	60.6	36.6	2.8	4.0
7.5% NiC10R7	6.6	58.9	38.2	2.9	4.8
7.5% NiC12R7	0.9	63	28.4	8.6	2.3
4% NiC8R6	4.5	83.5	14.0	2.5	1.9
4% NiC8R7	4.6	81.0	17.2	1.8	3.4
4% NiC8R8	3.8	69.4	28.4	2.2	4.1
1.5% NiC6R7(E)	2.3	87.9	9.3	2.8	3.4

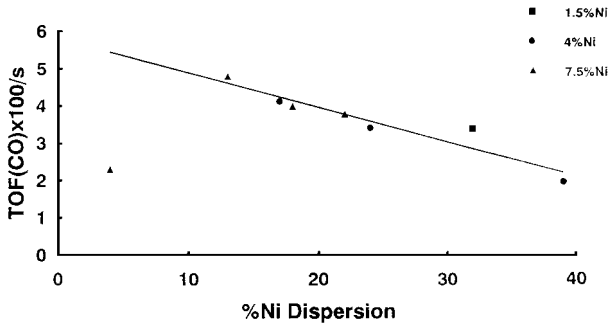

FIG. 4. CO turnover frequency (TOF) at 533 K versus the percentage of nickel dispersion. The straight line represents the linear fit to the experimental points, neglecting the one with the lowest dispersion.

The reported activity data were recorded after 2 h time on stream.

The selectivity toward heavier hydrocarbons, indicated by C_{2+} and consisting essentially of ethane and small amounts of propane, *n*-butane, and propene, is generally higher, as for nickel/silica catalysts operating under the same H_2/CO ratio and the same total pressure (15).

Specific activities in terms of turnover frequencies, TOF(CO), calculated as molecules of CO converted per catalytic site per second, are plotted versus metal dispersions in Fig. 4. With the exception of the sample with the largest particle size, decreasing TOF with increasing dispersion is generally observed, regardless of the preparation procedure and the metal concentration of the various catalysts. It is worth noting that the two sets of samples, those calcined at different temperature and those calcined at the same temperature, behave similarly, suggesting that the precursor treatment is not relevant. The decrease of the CO hydrogenation activity with increasing catalyst dispersion has been observed already for Ni on different supports (4, 40, 41). In one case the behavior was attributed to the interaction between metal and support, producing a modification in the nature of the stoichiometry of CO and H_2 adsorption (4). In the other case the decrease of activity with decreasing particle diameters observed with Ni particle sizes smaller than 60 Å was explained with the decrease of the number of ensembles (40). Changes of the activity with particle size have been also attributed to a lower activity on the high index planes of the smaller particles of Ni associated with a preferential buildup of carbon on these planes (41).

The methane turnover frequency (obtained by the TOF(CO) times the methane selectivity) is plotted versus the nickel dispersion in Fig. 5. Except for particle dispersion smaller than 4% and larger than 39%, in the range of dispersion between 10 and 35%, the turnover frequencies seem to be independent on the metal dispersion. In Fig. 6 the C_{2+} yield/CH_4 yield versus nickel dispersion is reported. The C_{2+} yield ratio decreases with increasing Ni

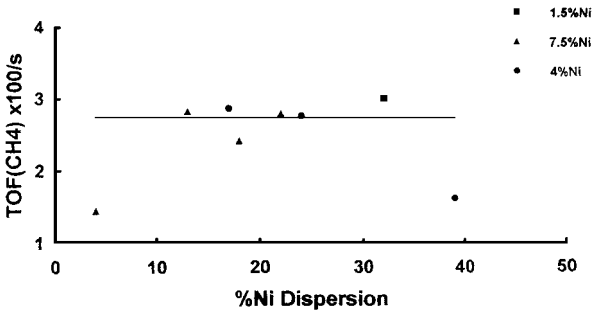

FIG. 5. CH_4 turnover frequency (TOF) at 533 K versus the percentage of nickel dispersion. The straight line represents the linear fit to the experimental points, neglecting those at the ends of the dispersion range.

dispersion until reaching a plateau at dispersion values above 25%. The same type of results have been described with Ni/SiO_2 catalysts at 488 K using $H_2/CO = 4$ (40). The decrease of selectivity with the increasing dispersion was attributed to the different ensemble sizes involved in the formation of methane and ethane. The larger ensembles required by the second reaction lead to a more pronounced effect of the particle sizes (42).

The opposite behavior is reported for the methanation reaction on Ni/SiO_2 and Ni/Al_2O_3 catalysts at 525 and 500 K, respectively, and with $H_2/CO = 4$. A decrease of the methane turnover frequencies and an increase of the C_{2+} yield/CH_4 yield ratio with increasing dispersion was indeed obtained (4). It was argued that, on the small nickel crystallites interacting strongly with the support, the adsorption of hydrogen was inhibited, resulting in the production of hydrogen-poor hydrocarbons. The nature of the support and, therefore, its interaction with the metal was found to affect the C_{2+} selectivity (3).

The much lower conversion rate exhibited by the catalyst 7.5% NiC12R7 is probably due to the incomplete reduction of the nickel, as revealed by the X-ray diffractogram. Moreover, the higher CO_2 selectivity cannot be considered as an indication of a different reaction pattern since the low level of conversion can imply a rather high uncertainty.

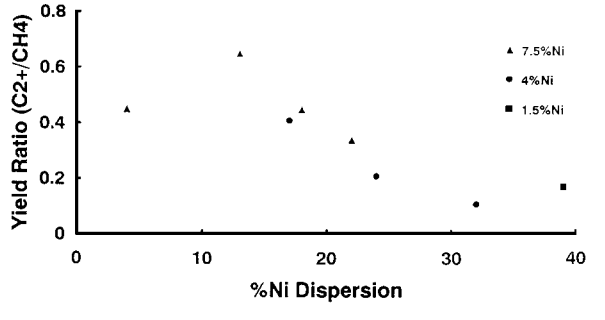

FIG. 6. Ratio of the C_{2+} hydrocarbon yield and CH_4 yield versus the percentage of nickel dispersion.

Recent studies on methanation reactions have shown that the dominant mechanism involves the dissociation of CO, followed by the hydrogenation of the surface carbon atoms to methane (43). The carbon activated on the catalyst surface then reacts progressively with the activated hydrogen in the following way:

$$C + H \Leftrightarrow CH + 3H \Leftrightarrow CH_2 + 2H \Leftrightarrow CH_3 + H \Leftrightarrow CH_4\uparrow.$$

Such a reaction depends on the hydrogen coverage and competes with the reaction occurring between the adsorbed intermediate carbon species forming higher molecular weight hydrocarbons.

Several studies have shown that during CO hydrogenation over transition-metal surfaces, the presence of alkali ions increases the selectivity to C_{2+} hydrocarbons (15, 44). Molecular orbital calculations for CO chemisorbed on Ni(100), indicated that the 5σ orbital electrons of CO interact with the $3d_{z^2}$ orbital of nickel and that a back-donation to the antibonding 2π orbital from the filled density of electron states of the metal occurs (45).

An electron donor capability, due to the presence of the alkali ions, was also found in pumice, as demonstrated in a series of palladium catalysts (26, 46). However, a recent IR study of CO adsorption on Pd, supported on synthetic pumices, with variable Na/Pd atomic ratios ranging from 2 to 6, showed that a decreased intensity along with a downfield shift of the CO stretching frequency was not accompanied by dissociation of CO, which is different from the surface alkali ion-doped Pd/silica catalysts (27). In the present case, where the bulk atomic ratio (K + Na)/Ni ranges from 1 to 5, treatment at a temperature above 673 K, produces surface segregation of the alkali ions according to previous XPS study of Ni/pumice (28). This would contribute to a further weakening of the C–O bond because of the possible formation of a $Ni–C–O^-Na^+$ species. Consequently, an increase of the C_{2+} selectivity, as compared to undoped nickel/silica catalysts used in the same reaction under the same experimental conditions of the present study, would result (15). If the electronic effects are expected to increase with increasing catalyst dispersion, weakening the C–O bond (26), on the other hand, the geometric effect on a metal particle decorated by the alkali ions, by modifying the required ensemble for the adsorption and dissociation of CO, may determine, as in the present case, a decrease of the C_{2+} selectivity with increasing metal dispersion. In this case the particle size-dependence would be due to a sort of dilution effect played by the alkali ions, rather than a simple decrease of the number of ensembles (40).

The decrease of the CO conversion rate (Fig. 4) and the invariance of the methane formation rate (Fig. 5) with the Ni dispersion suggest that the rate-determining step for the methane formation is the hydrogenation of the carbon atom. As shown from the structural study of the catalyst precursors, the interaction between the metal and support

is not very strong, at least in the range of the calcination temperatures used. Consequently, the hydrogen adsorption capability may not be affected by the changing size. On the contrary, given the particle size dependence of the C_{2+} selectivity, the adsorption and dissociation of CO are rate-determining in the production of C_{2+}. A combination of long-range and local electronic effects played by the alkali ions determines the adsorption and subsequent dissociation of CO with the observed superior C_{2+} selectivity as for Ni/SiO_2 catalysts. However, the particle size dependence should be ascribed essentially to the dilution effect of the alkali ions.

From the steady state CO conversion rate as a function of temperature, typically a value of 22 kcal/mole for the activation energy was obtained, comparable to the value from Ni/SiO_2 prepared by incipient wetness impregnation (41).

The stability of the Ni/pumice catalysts in the CO hydrogenation has been evaluated by performing a series of tests lasting 14–18 h. A typical plot of such a stability test referred to the 4NiC8R8 catalyst in terms of CO conversion versus reaction time is shown in Fig. 7. The Ni/pumice catalysts denoted an excellent stability since a decay in the activity lower than 5% of the initial value after 14 h time on stream was noticed. The X-ray diffraction analysis of the samples, after being used in the reaction, excluded the occurrence of metal sintering. The same XPS intensity ratios of the Ni 2p over Si 2p, obtained for samples before and after the reaction, agreed with this conclusion.

The XPS of the C 1s core level in the catalyst 7.5% NiC8R7, before and after reaction, shown in Fig. 8, are essentially the same. No changes are observed in the binding energies and, also, in the relative and total amounts of the carbon species. Fitting of the spectra gives one main component at 284.6 eV due to the adventitious carbon used as the binding energy reference and two additional peaks between 286 and 289 eV due to more oxidized carbons formed, even at room temperature in air. Carbidic carbon, usually considered a precursor in the coke formation was absent in the C 1s spectrum after the reaction.

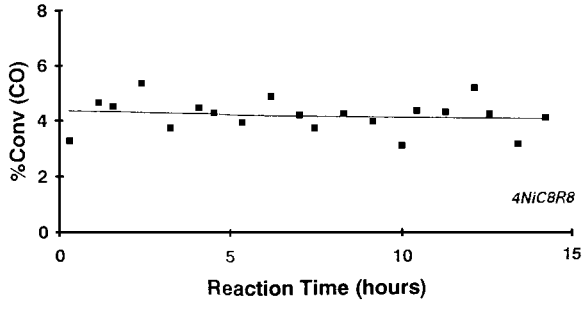

FIG. 7. Percentage of CO conversion versus time over the 4NiC8R8 catalyst.

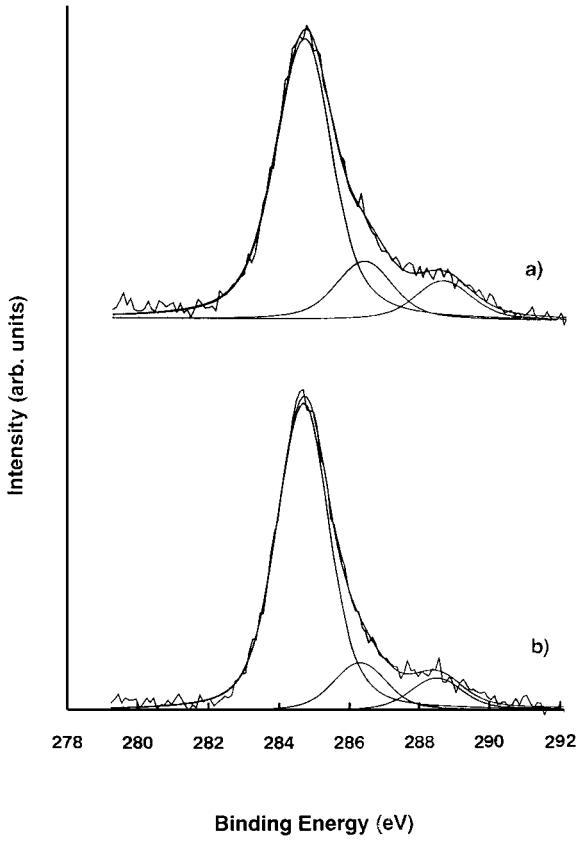

FIG. 8. X-ray photoelectron spectra of C 1s levels: (a) 7.5% NiC8R7 before the reaction and (b) 7.5% NiC8R7 after the reaction.

CONCLUSION

The effect of calcination and reduction temperatures on the structural properties of the oxide precursors and of the reduced catalysts indicated a weak chemical interaction between the Ni(II) species and the pumice support elements. Stronger interactions are formed at high calcination temperatures, resulting in oxide species that are more difficult to reduce. The selectivity of such catalysts toward heavier hydrocarbons is generally higher, as compared to undoped nickel silica catalysts. The TOF of the CO conversion decreases with increasing catalyst dispersion, following a distinct trend, regardless of any differences in the catalyst preparation or thermal treatments. A parallelism between the CO conversion activity and the C_{2+} selectivity versus the nickel particle dispersion indicated that the same factors affect both. When the particle size decreases, a dilution effect, probably due to surface segregation of alkali ions naturally present in the structure of pumice reduces the chemisorption of CO and its dissociation rate, producing a decrease in both activity and C_{2+} selectivity. The invariance of the methanation activity with the particle size indicates that the hydrogenation of the carbon, probably the rate determining step for the methanation process, is insensitive

to the particle size, suggesting once more that the metal–support interaction, which usually inhibits the adsorption of hydrogen, is rather weak.

The catalysts do not undergo nickel sintering during the CO hydrogenation reaction. The performance of the catalysts is practically constant over a period of 14 h. This is in agreement with the absence of any carbidic carbon in the C 1s photoelectron spectra of a catalyst after the reaction.

ACKNOWLEDGMENTS

We thank the Consiglio Nazionale delle Ricerche (CNR) (Progetto Strategico "Tecnologie Chimiche Innovative") and MURST (40%) for financial support.

REFERENCES

1. Kelley, R. D., and Goodman, D. W., *Surf. Sci.* **123**, L743 (1982).
2. Goodman, D. W., *Accts. Chem. Res.* **17**, 194 (1984).
3. Vannice, M. A., and Garten, R. I., *J. Catal.* **56**, 236 (1979).
4. Bartholomew, C. M., Pannell, R. B., and Butler, J. L., *J. Catal.* **65**, 335 (1980).
5. Gil, A., Diaz, A., Gandia, L. M., and Montes, M., *Appl. Catal. A* **109**, 167 (1994).
6. Pajonk, G. M., and Teichner, S. J., *Stud. Surf. Sci. Catal.* **27**, 277 (1986).
7. Tauster, S. J., and Fung, S. C., *J. Catal.* **55**, 29 (1978).
8. Somorjai, G. A., *in* "Introduction to Surface Chemistry and Catalysts." Wiley, New York, 1993.
9. Praliaud, H., Delmon, J. A., Mirodatos, C., and Martin, C. A., *J. Catal.* **97**, 344 (1986).
10. Brum Pereira, E., and Martin, G. A., *Appl. Catal. A* **103**, 291 (1993).
11. Mirodatos, C., Brum Pereira, E., Gomez Cobo, A., Dalmon, J. A., and Martin, G. A., *Topics Catal.* **2**, 183 (1995).
12. Mate, C. M., Kao, C. T., and Somorjai, G. A., *Surf. Sci.* **206**, 145 (1988).
13. Crowell, J. E., Tysoe, W. T., and Somorjai, G. A., *J. Phys. Chem.* **89**, 1598 (1985).
14. Bartholomew, C. H., *Stud. Surf. Sci. Catal.* **64**, 158 (1991).
15. Pereira, E. B., and Martin, G. A., *Appl. Catal. A* **115**, 135 (1994).
16. Rostrup-Nielsen, J. R., *J. Catal.* **85**, 31 (1984).
17. Bernardo, C. A., Alstrup, I., and Nielsen, J. R., *J. Catal.* **96**, 517 (1985).
18. Tavares, M. T., Alstruyp, I., Bernardo, C. A., and Rostrup-Nielsen, J. R., *J. Catal.* **158**, 402 (1996).
19. Alstrup, I., *J. Catal.* **151**, 216 (1995).
20. Alstrup, I., *J. Catal.* **109**, 241 (1988).
21. Fagherazzi, G., Benedetti, A., Deganello, G., Duca, D., Martorana, A., and Spoto, G., *J. Catal.* **150**, 177 (1994).
22. Venezia, A. M., Duca, D., Floriano, M. A., Deganello, G., and Rossi, A., *Surf. Interface Anal.* **19**, 543 (1992).
23. Deganello, G., Duca, D., Martorana, A., Fagherazzi, G., and Benedetti, A., *J. Catal.* **150**, 127 (1994).
24. Duca, D., Liotta, L. F., and Deganello, G., *J. Catal.* **154**, 69 (1995).
25. Duca, D., Frusteri, F., Parmaliana, A., and Deganello, G., *J. Catal.* **146**, 269 (1996).
26. Venezia, A. M., Rossi, A., Duca, D., Martorana, A., and Deganello, G., *Appl. Catal. A* **125**, 113 (1995).
27. Liotta, L. F., Martin, G. A., and Deganello, G., *J. Catal.* **164**, 000 (1996).
28. Venezia, A. M., Bertoncello, R., and Deganello, G., *Surf. Interface Anal.* **23**, 239 (1995).
29. Van Dillen, J. A., Geus, J. W., Hermans, L. A. M., and Van der Mejden, J., *in* "Proc. 6th International Congress on Catalysis, London, 1976" (G. C. Bond, P. B. Wells, and F. C. Tompkins, Eds.), p. 677. Chemical Society, London, 1976.
30. Klug, H. P., and Alexander, L. E., "X-ray Diffraction Procedures for Polycrystalline and Amorphous Materials," Wiley, New York, 1954.
31. Smith, J. S., Thrower, P. A., and Vannice, M. A., *J. Catal.* **68**, 270 (1981).
32. Mustard, D. G., and Bartholomew, C. H., *J. Catal.* **67**, 186 (1981).
33. Tamagawa, H., Oyama, K., Yamaguchi, T., Tanaka, H., Tsuiki, H., and Ueno, A., *J. Chem. Soc. Faraday Trans. I* **83**, 3189 (1987).
34. Mile, B., Stirling, D., Zammitt, M. A., Lovell, A., and Webb, M., *J. Catal.* **114**, 217 (1988).
35. Roman, A., and Delmon, B., *J. Catal.* **30**, 333 (1973).
36. Zielinski, J., *J. Catal.* **76**, 157 (1982).
37. Balerna, A., and Mobilio, S., *Phys. Rev. B* **34**, 2293 (1986).
38. Kuroda, H., Yokoyama, T., Asakura, K., and Iwasawa, Y., *Faraday Discuss.* **92**, 189 (1991).
39. Mott, N. F., and Littleton, M. J., *Trans. Faraday Soc.* **34**, 485 (1938).
40. Dalmon, J-A., and Martin, G. A., *in* "Proc. 7th Int. Cong. Catal., Tokyo, 1980," p. 402. Kodanska, Tokyo, 1981.
41. Lee, C., Schmidt, L. D., Moulder, J. F., and Rusch, T. W., *J. Catal.* **99**, 472 (1986).
42. Martin, G. A., *Catal. Rev.-Sci. Eng.* **30**, 519 (1988).
43. Guczi, L., *Stud. Surf. Sci. Catal.* **64**, 350 (1991).
44. Crowell, J. E., Tysoe, W. T., and Somorjai, G. A., *J. Phys. Chem.* **89**, 1598 (1985).
45. Wimmer, E., Fu, C. L., and Freeman, A. J., *Phys. Rev. Lett.* **55**, 2618 (1985).
46. Venezia, A. M., Rossi, A., Liotta, L. F., Martorana, A., and Deganello, G., *Appl. Catal. A* **147**, 81 (1996).